Usage Report for Fiscal Year 2024

Project Title: Collective properties of self-propelled particles: Diffusion and Non-equilibrium phenomenon

Name: Franco Nori (1,2) and Pulak Kumar Ghosh (1,3)

(1) Theoretical Quantum Physics Laboratory, RIKEN Cluster for Pioneering Research, Wakoshi, Saitama 351-0198, Japan.

(2) Department of Physics, University of Michigan, Ann Arbor, Michigan 48109-1040,USA

(3) Department of Chemistry, Presidency University, 86/1 College Street, Kolkata, 700073, India.

Laboratory at RIKEN:

Theoretical Quantum Physics Laboratory, RIKEN Cluster for Pioneering Research, Wako-shi, Saitama 351-0198, Japan

1. Background and purpose of the project, relationship of the project with other projects

The normal diffusion of an ideal massless Brownian particle is usually associated with the Gaussian distribution of its spatial displacements. However, there are no fundamental reasons why the diffusion of a physical Brownian tracer should be of the Fickian type[1]. For instance, displacement distributions in real biophysical systems appear to retain prominent exponential tails, even after the tracer has attained the condition of normal diffusion. Such an effect, often termed non-Gaussian normal diffusion (NGND), disappears only for exceedingly long observation times (possibly inaccessible to real experiments [1]), when the tracer's displacement distribution eventually turns Gaussian, as dictated by the central limit theorem. Persistent diffusive transients of this type have been detected in experimental and numerical setups. The signature of NGND, along with a non-Gaussian velocity distribution, has been previously reported in systems with spatial heterogeneity. The current interpretation of such diverse NGND manifestations as transient effects postulates the existence of one or more slowly fluctuating processes affecting composition, geometry, and dynamics of the tracer's environment.

When investigated collectively, a suspension of active particles may undergo phase separation even in the absence of cohesive forces [2-3]. The ensuing motility-induced phase separation (MIPS) is arguably the simplest nontrivial collective feature that distinguishes active from passive particles [30]. MIPS involves the coexistence of two active phases of different densities, similarly to what happens in a binary fluid mixture below its critical temperature. It occurs as a combined effect of steric interactions and self-propulsion, even in the absence of pair alignment, interactions with solid substrates, or thermal fluctuations [2-3]. Experimental evidence of MIPS has been obtained both in biological and synthetic systems, despite numerous technical difficulties. Among the quantitative tools employed to numerically characterize MIPS, diffusivity offers arguably the most direct access to the microscopic dynamics underlying phase separation. The asymptotic diffusion constant has been computed as an overall indicator of both gas-liquid [2] and liquid-solid separation [4]. Diffusivity was utilized also to analyze the inner structure of the separating clusters [3].

We have demonstrated that diffusion in an athermal active suspension under MIPS may provide a more predictive tool than previously reported. To avoid more complex phase diagrams, we restrict our investigation to a two-dimensional (2D) suspension of active hard disks. Such disks undergo normal diffusion no matter what the suspension phase. Upon increasing the suspension packing fraction with uniform initial particle distribution, the

diffusion constant exhibits a sharp drop, which we interpret as the gaseous phase spinodal. However, slowly ramping up and down the overall packing fraction, produces a robust hysteresis loop delimited by the binodal and spinodal of the gaseous phase. Vice versa, within our numerical accuracy, the binodal region of the dense phase appears to collapse, so that no hysteretic diffusion loop was observed. Moreover, in the presence of MIPS, the corresponding particle displacement distributions are leptokurtic for extended time transients (i.e., tend to zero slower than a Gaussian function), a clear-cut NGND manifestation.

2. Specific usage status of the system and calculation method

This fiscal year, we used the Hokusai supercomputer mainly for numerically studying diffusion transients associated in motility-induced phase separation. To be specific, we focus to determine spinodal points and binodal regions using self-diffusion as a tool. Details of our simulation results are presented in the next section. We employed the following methods to explore intriguing features of motility-induced phase separation (MIPS).

Theoretical and simulation method

We simulated a two-dimensional suspension of N identical achiral active Janus particles [5] modeled as disks of radius r_0 and constant self-propulsion speed v_0, in a square box of size L with periodic boundary conditions. The dynamics of a single JP of coordinates r = (x, y) obeys the simple Langevin equations,

$$\mathbf{r}_i = \mathbf{v}_0;\ \ \dot{\theta}_i = \sqrt{D_\theta}\zeta_i^\theta(t) \quad - - - - - (2)$$

Here, the orientation of the self-propulsion vector $\mathbf{v_0}$ $=v_0(\cos\theta, \sin\theta)$, measured with respect to the longitudinal x-axis, fluctuates subjected to the stationary, delta-correlated noise source $\xi_\theta(t)$, with $\langle\xi_\theta(t)\xi_\theta(0)\rangle=2\delta(t)$. Following Ref. [2], the suspension is assumed to be athermal, that is, we neglect thermal fluctuations against the angular noise intrinsic to the self-propulsion mechanism [6-9]. The reciprocal of D_θ defines the correlation time, τ_θ , and the persistence length, $l_\theta = v_0/D_\theta$ of a free self-propelled Janus particle (JP). For $t >> \tau_\theta$ a free JP would undergo normal diffusion with diffusion constant $Ds = v^2_0/2D_\theta$, but non-Gaussian statistics. We assume that at short distance the disks repel each other via the truncated Lennard-Jones potential.

The coupled stochastic differential equations (2) were numerically integrated by means of a standard Milstein scheme to obtain particle position as a function of time. Then, we numerically calculated local density distribution, packing fraction of the different phases, transition points (spinodal and binodal), self-diffusivity of the particles, and displacement distribution. The numerical integration was carried out using a very small time step, 10^{-3} -10^{-4} to ensure numerical stability. We assume initially that the particles were randomly distributed in the simulation box with random orientation of the self-propulsion velocities. Mean square displacement, P(x,t), and the diffusion coefficient here were obtained by averaging over 104 trajectories. One part of this project has been completed, and the results have been published. However, additional simulation work is necessary to understand the related features mentioned in the future plan.

3. Results

Self-diffusion and motility induced phase-separation -- To characterize the underlying features of MIPS, we choose particles self-diffusion as a quantifier. We simulated mean square displacement as a function of time, and from there, we extracted the diffusion constant in the long time limit. This constant is a function of the average packing fraction of the system. A sudden diffusivity drop marks phase separation. This MIPS signature is sharp enough to determine gas spinodal as a function of self-propulsion velocity. As apparent in Figs. 1(b), 1(c), 2(c), and 2(d), no MIPS occurs for v0

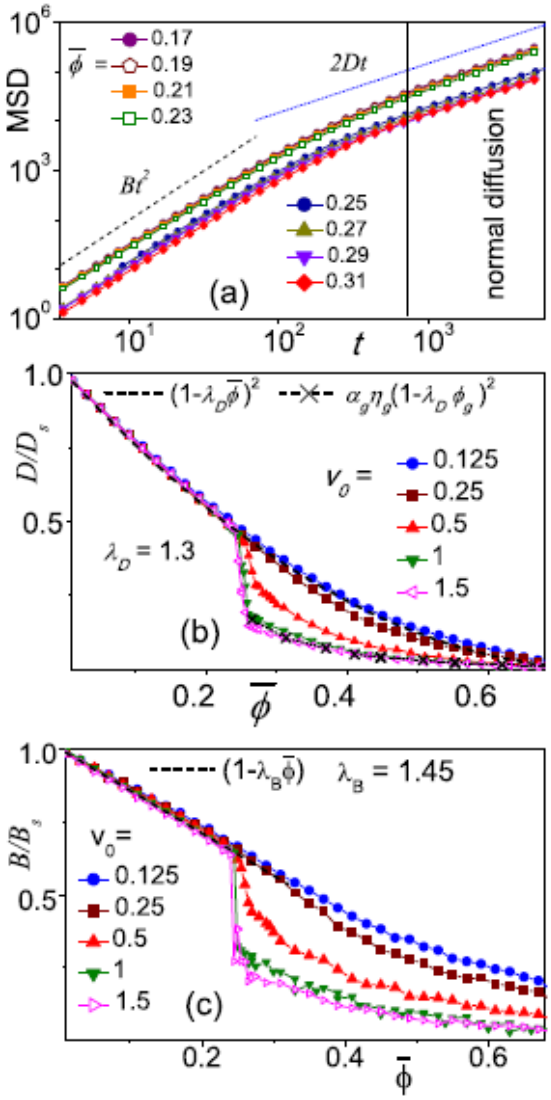

Fig1: Particle mean-square displacement (MSD) in a suspensions of N active JP's of radius $r_0 = 1$ and persistence time $\tau_\theta = 100$; N = 9120. Packing fraction $\bar{\varphi}$ (defined as $\pi r_0^2 N/L^2$) was varied by tuning simulation box size at fixed N. If not stated otherwise, the suspension was initially randomly uniform. (a) MSD, $\langle \Delta x^2 \rangle$, vs t for v0 = 1 and different $\bar{\varphi}$. The short-time ballistic and the asymptotic diffusive branches are fitted respectively by quadratic, Bt2, and linear, 2Dt, functions. The fitting parameters D (in units of $D_s = v^2_0/2D_\theta$) are plotted in (b) vs $\bar{\varphi}$. The fitting parameters B (in units of $B_s = v^2_0/2$) vs $\bar{\varphi}$ with different v_0 (see legend) are plotted in (c). The dashed lines in (b) and (c) depicting the $\bar{\varphi}$ dependence of D/D_s and B/B_s (for $v_0 = 1$) are fitted by the functions in the legends. Crosses in (b) display Eq. (2).

below a critical value, $v_0^* < 0.25$, while for $v_0 > v_0^*$ the dependence of φ_* on v_0 is rather weak. Similarly, Fig. 2(d) shows that for a given v_0 there exists an upper bound for the angular diffusion constant $D\theta$, above which MIPS does not occur.

In the homogeneous phase, the fitting ballistic, B, and diffusion, D, constants of Fig. 1(a) appear to slowly decrease with increasing $\bar{\varphi}$ up to the MIPS onset, $\bar{\varphi} = \varphi_*$. Standard stoichiometric arguments suggest polynomial fitting laws,

$$D = D_s(1 - \lambda_D\bar{\varphi})^2 \text{ and } B = B_s(1 - \lambda_B\bar{\varphi}) \quad ---(2)$$

with $D_s = v_0^2/2D_\theta$ and $B_s = v_0^2/2$. Both fitting parameters λB [in Fig. 1(c)] and λD [in Fig. 1(b)] are larger than the reciprocal of the close-collisional packing fraction, $\varphi cp = p/4$. MIPS drops of the curves $B(\bar{\varphi})$ are apparent, in quantitative agreement with the existence of a critical value v_0^*, below which MIPS is ruled out [see Figs. 2(c) and 2(d)].

To analyze the tails of $D(\bar{\varphi})$ for $\bar{\varphi} > \varphi_*$, we had recourse to the two-phase characterization of Figs. 2(a) and 2(b) (also for $v_0 = 1$). After exceedingly long simulation runs, $t = 10^5$, the dense and dilute phases of the suspension appear to be well separated. We computed the volume, α_i, and number, h_i, fractions of both phases and the resulting phase packing fractions, i (i = g, c denoting, respectively, the gaseous and the dense phases). To this purpose we first computed the corresponding phase densities ρ_i, by selecting rectangular regions (as large as possible) within either phases and then counting particles in there. This procedure was repeated 10 times for different "trajectories," namely initial configurations and random number sequences. This way we estimated the phase mean densities as well as their standard deviations (under the simplifying assumption that both phases were homogeneous). Finally, we computed the phase areas, A^i, by imposing the two normalization conditions $\rho_c A_c + \rho_g A_g = N$ and $A_c + A_g = L^2$.

By definition, $\varphi_i = \bar{\varphi}\frac{\eta_i}{\alpha_i}$, as numerically checked in Fig. 2(a). The densities of the two phases are

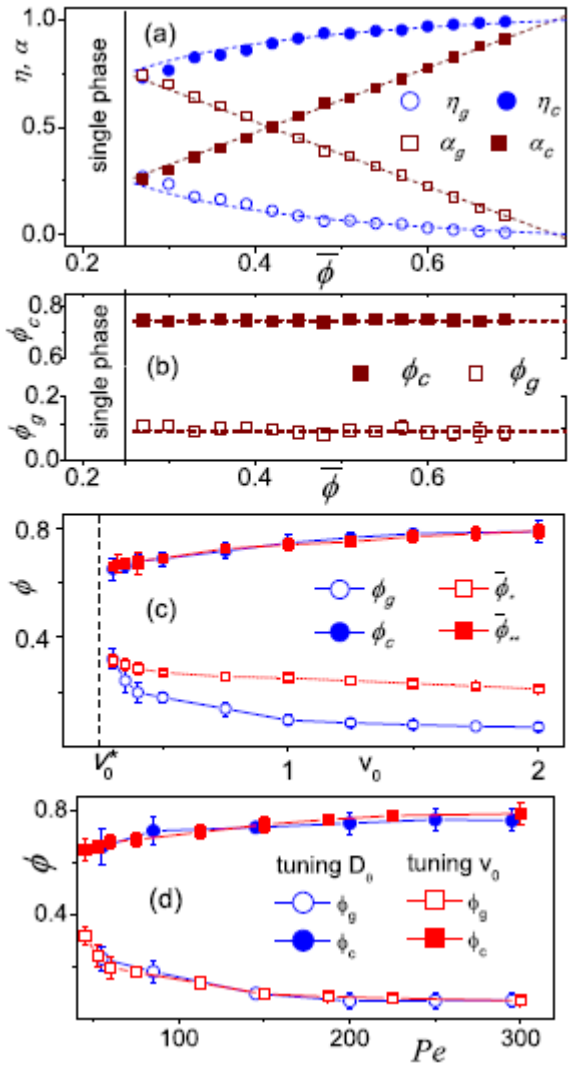

FIG.2. Gaseous and dense phases (denoted respectively by the indices i = g, c): $\bar{\varphi}$ dependence of (a) the phase number, η_i, and volume, α_i, fractions and (b) the phase packing fractions, φ_i, for $N = 10^4$, $v_0 = 1$, $\tau_\theta = 100$, and random uniform initial conditions. As a consistency test, we fitted the data for α_i and φ_i with straight lines [dashed lines respectively in (a) and (b)] and made use of the identity, $\varphi_i = \bar{\varphi}\frac{\eta_i}{\alpha_i}$, to reproduce the φ^- dependence of η_i in (a). Fitting functions: $\alpha_c = 1.5\bar{\varphi} - 0.14$, $\varphi_c = 0.75$, and $\varphi_g = 0.09$. Recall that $\alpha_g + \alpha_c = 1$ and $\eta_g + \eta_c = 1$. (c) Cluster, φ_c, gaseous phase, φ_g, and MIPS onset, φ_* and φ_{**}, packing fractions vs v_0 for $\bar{\varphi} = 0.45$. For $v_0 < v_0^*$ MIPS never occurs, while for $v_0 > v_0^*$ our data suggest that $\varphi_c^{(s)} + \varphi_g^{(s)} = 1$. (d) Gaseous and cluster phase binodal, φ_g and φ_c, vs $Pe = 3v_0/(2r_0D_\theta)$ for N = 9, 120, $v_0 = 1$(blue symbols), and $D_\theta = 10^{-2}$ (red symbols).

confirmed to be independent of $\bar{\varphi}$. On neglecting the contribution from the particles trapped in the cluster, the self-diffusion constant for $\bar{\varphi} > \varphi_*$ can be approximated to [10],

$$D_{MIPS}(\bar{\varphi}) = \alpha_g D_g \eta_g (1 - \lambda_D \varphi_g)^2$$

Here, we made use of the fact that the gaseous phase represents a fraction η_g of the suspension and behaves as a homogeneous phase with low packing fraction φ_g and fractional volume α_g. A comparison with the actual D data for $v_0 = 1$ is displayed in Fig. 1(b).

(2) Hysteresis loops: spinodal and binodal points

By starting with a uniform particle distribution we never observed MIPS in the range $\bar{\varphi} \in [\varphi_g, \varphi_*]$, regardless of the (accessible) running time. The outcome changed when we slowly increased (decreased) $\bar{\varphi}$ over time. We did so by keeping N fixed and decreasing (increasing) L stepwise after a fixed long running time t (typically $t = 5 \times 104$). Upon varying L, we rescaled the suspension configuration accordingly. This produced the hysteresis loops of Fig. 3(a), which, for large N, approach the ideal loop obtained by connecting the fitting functions of D vs $\bar{\varphi}$ in Fig. 1(b) [also see Eqs. (3) and (4)]. On increasing $\bar{\varphi}$, MIPS occurs, as anticipated above, at $\bar{\varphi}$ (signaled by a D drop), but upon decreasing it only disappears for $\bar{\varphi} \geq \varphi_g$ (signaled by a fast D rise).

To check robustness of the hysteretic effect toward translational noises, we simulate Eq. (1) after adding a 2D translational Gaussian noise term with strength D_0. . The hysteresis loop of Fig. 3(a) there turned out to be quite robust; indeed, it appeared to vanish only for D_0 of the order of D_s. Vice versa, its area may be quite sensitive to the suspension size, N

Recall that our hysteresis protocol $\bar{\varphi}$ was increased/decreased stepwise at regular time intervals t. Of course, we cannot rule out the possibility that the resulting hysteresis loop shrinks and finally disappears for exceedingly large t (in any case, well beyond our computing capabilities). Similar remarks apply to even simpler dynamically

bistable systems, such as the motility of a weakly damped, driven Brownian particle confined to a one-dimensional washboard potential. For the suspension of Fig. 3(a), we repeatedly looped $\bar{\varphi}$ in the range (0.05, 0.30), that is, across the relevant binodal and spinodal of the gaseous phase.

As we verified that the hysteretic effect is robust toward translational noises, it has also been noticed that hysteresis loops become sharper upon increasing the suspension size, N, and the observation time, t. In conclusion, accurate data for the D(φ) hysteresis loop suffice to self-consistently characterize the gaseous binodal region at fixed v_0. Further, the persistence of uniformly distributed short-time aggregates in the suspensions with $\bar{\varphi} \leq \varphi_*$, suggests interpreting $\bar{\varphi}$ as the gaseous phase spinodal, $\bar{\varphi} = \varphi_g^{(s)}$.

A similar approach was adopted by simulating initially homogeneous, dense suspensions and decreasing $\bar{\varphi}$ below φ_c: at a sufficiently low value of the overall packing fraction, $\bar{\varphi} = \varphi_{**} < \varphi_c$, the dense suspension developed coalescing gaseous bubbles. Therefore, the curve φ_{**} versus v_0 displayed in Fig. 2(c) is our best estimate of the cluster spinodal, $\varphi_c^{(s)}$. As illustrated in Fig. 3(b), at $\bar{\varphi} = \varphi_c^{(s)}$, the curves D versus $\bar{\varphi}$ exhibit a second drop, though not as sharp as at $\bar{\varphi} = \varphi_g^{(s)}$, but no hysteretic loop. In fact, cluster binodal and spinodal curves. run so close to one another that we could hardly separate them; the upper binodal region appears to collapse (see Ref. for an analytical treatment). Remarkably enough, our numerical data suggest that $\varphi_c^{(s)} + \varphi_g^{(s)} = 1$. As v_0 approaches v_0^* (from above), both upper and lower pairs of binodal and spinodal curves overlap (for details see []).

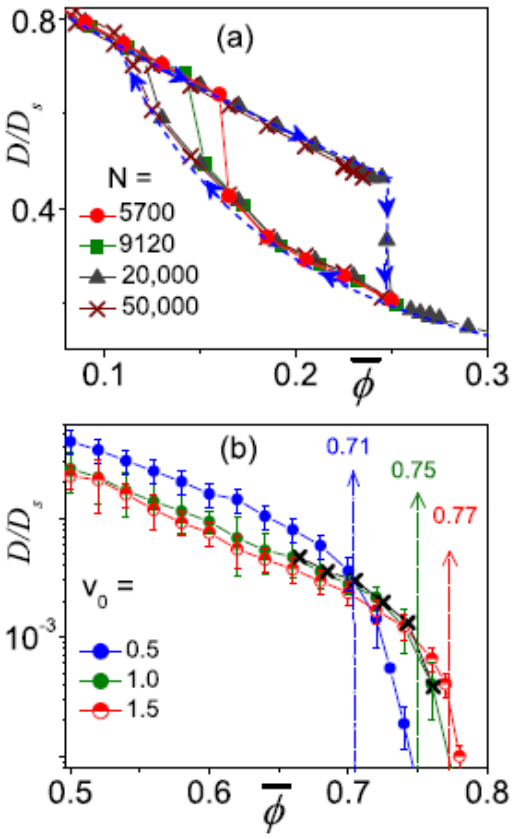

FIG. 3. (a) Hysteresis loop obtained by slowly ramping $\bar{\varphi}$ up and down across the gaseous binodal-spinodal range for $v_0 = 1$ with different N (see legends). The reference hysteresis loop (dashed blue curve) has been closed by extending the lower fitting curve, $D_{MIPS}(\bar{\varphi})$, in Fig. 1(b) down to $\bar{\varphi} = \varphi_g$. (b) D vs $\bar{\varphi}$ in the upper binodal region for different v0 and N = 20 000. For $v_0 = 1$, D was determined as in (a), by ramping $\bar{\varphi}$ up (dots) and down (crosses); no hysteresis loop was detected, as the upper binodal region appears to collapse.

4. Conclusion

We characterized MIPS of an athermal, achiral active suspension by looking at the particle diffusivity under steady-state conditions. The choice of using the overall suspension packing fraction as tunable parameter has a practical motivation, as in most applications the particle motility cannot be varied at will, while their density can. Particle diffusion under phase separation has been proven to show hysteretic and NGND properties. Our main conclusions are (1) The hysteresis loop of the curve D(φ) in the lower binodal region, which allows a direct measure of φ_g and $\varphi_g^{(s)}$.

(2) The peculiar properties of the upper binodal and spinodal curves, which appear to overlap, thus suppressing hysteresis in the upper binodal region. Our numerical data also suggest a mirror symmetry of the spinodal curves with $\varphi_c^{(s)} + \varphi_g^{(s)} =$

1.

(3) Non-Gaussian normal diffusion characterized motility induced phase separation with leptokurtic transient distributions of displacements x. The associated NGND transient time is almost four orders of magnitude larger than the rotational relaxation time of a free JP. Further, we show that NGND characterized MIPS also in the presence of hysteresis

5. Schedule and prospect for the future

In the upcoming fiscal year, we intend to investigate issues that emerged during the current fiscal year's research work. Our detail analysis of motility induced phase separation [Phys.Rev.Research 7, 013153 (2025)] raised the following issues:

(a) When the system's average packing fraction crosses the critical threshold known as the spinodal point, a large single cluster is formed in the thermodynamic limit. However, distinguishable phases can be easily achieved when the self-propelled velocity and persistence length (or, alternatively, the Péclet number) are much larger than their critical threshold values. The structure around the critical velocity (v_0*) or Péclet number (Pe*) is not well understood. Even over long time periods, small clusters do not collapse into a single large cluster. To gain a better understanding of the structure and dynamics near the transition point, we plan to numerically calculate the number of clusters and their sizes as a function of time. Additionally, we will analyze density fluctuations and the structure factor to characterize the structural heterogeneity.

(b) Most previous studies on motility-induced phase separation have focused on systems of active swimmers where all the particles have the same self-propulsion velocity, persistence length, and intrinsic torque. However, in both artificial and natural systems, while individual particles may be similar, their self-propulsion properties can vary. Considering such realistic situations, we aim to explore the motility-induced phase separation (MIPS) properties of a system consisting of different types of self-propelled particles. Specifically, we will examine a system where self-propulsion velocity, intrinsic torque, and rotational diffusion are distributed over a range.

(c) Despite considerable effort, the structure and diffusion of systems with active particles remain poorly understood. To explain the experimentally observed features of various natural micro-swimmers, different types of interactions have been proposed. Recently, researchers have suggested that non-reciprocal interactions among the particles could help explain the collective behaviors of these micro-swimmers. Preliminary studies indicate that both the dynamics and structural mechanisms are significantly influenced by the nature of these non-reciprocal interactions. Building on previous research regarding non-reciprocally interacting active particles, we plan to explore a protocol in which individuals adjust their chirality by sensing the particles around them.

To address the issues mentioned above, we will utilize the numerical methods described in Section 2. We request an extension of our access to the computation facilities for the next usage term, continuing until March 31, 2026, under the same user category and project title.

6. References

[1] B. Wang, S. M. Anthony, S. C. Bae, and S. Granick, Proc. Natl. Acad. Sci. USA 106, 15160 (2009).

[2] Y. Fily and M. C. Marchetti, Phys. Rev. Lett. 108, 235702 (2012).

[3] G. S. Redner, M. F. Hagan, and A. Baskaran, Phys. Rev. Lett. 110, 055701 (2013).

[4] J. Bialké, T. Speck, and H. Löwen, Phys. Rev. Lett. 108, 168301 (2012).

[5] S. Jiang, S. Granick (Eds.), Janus particle synthesis, self-assembly and applications (RSC Publishing, Cambridge, 2012).

[6] P. K. Ghosh, V. R. Misko, F. Marchesoni and F. Nori, Phys. Rev. Lett., 2013, 110, 268301.

[7] P. K. Ghosh, P. Hänggi, F. Marchesoni and F. Nori, Phys. Rev. E, 2014, 89, 062115.

[8] P. K. Ghosh, Y. Li, F. Marchesoni, and F. Nori, Phys. Rev. E, 2015, 92, 012114.

[9] P. K. Ghosh, F. Marchesoni, Y. Li and F. Nori, Phys. Chem. Chem. Phys, 2021, 23, 11944-11953.

[10] S. Nayak, P. Bag, P. K. Ghosh, Y. Li, Y. Zhou, Q. Yin, F. Marchesoni, F. Nori, Phys. Rev. Research 7, 013153 (2025).

Fiscal Year 2024List of Publications Resulting from the Use of the supercomputer

S. Nayak, P. Bag, P. K. Ghosh, Y. Li, Y.　Zhou, Q. Yin, F. Marchesoni, F. Nori,
Diffusion transients in motility-induced phase separation
Physical Review Research 7 (1), 013153 (2025).
Date of Publication: 12 February 2025

[Paper accepted by a journal]

None

[Conference Proceedings]

None

[Oral presentation]

None

[Poster presentation]

None

[Others (Book, Press release, etc.)]

None